## Supporting Information

# "Sacrificial Protection in Action!"- Ultra-High Stability in Palladesite Mineral towards Oxygen Reduction Reaction

Saurav Ch. Sarma, Vamseedhara Vemuri, Vidyanshu Mishra, Sebastian C. Peter*
New Chemistry Unit, Jawaharlal Nehru Centre for Advanced Scientific Research, Bangalore 560064, India
*E-mail: sebastiancp@gmail.com, sebastiancp@jncasr.ac.in

---

## Experimental Methods

### S1. Chemicals

Palladium acetylacetonate ($Pd(C_5H_7O_2)_2$, 99%), selenous acid ($H_2SeO_3$, 98%), sodium borohydride ($NaBH_4$) and Nafion binder (5 wt%) were purchased from Sigma-Aldrich. Polyvinyl pyrrolidone (PVP) and tetraethylene glycol ($C_8H_{18}O_5$) were purchased from SDFCL and Alfa Aesar, respectively. All the reagents were used without further purification. Deionized water (TKA, 18.2 MΩ.cm) was used throughout the syntheses and measurements.

### S2. Synthesis of $Pd_{17}Se_{15}$ nanoparticles:

$Pd_{17}Se_{15}$ nanoparticles were synthesized by polyol synthesis method. $Pd(acac)_2$ (0.09 mmol) and 0.108 mmol $H_2SeO_3$ (0.1 mmol) were mixed together in 15 ml TEG in a 50 ml two-necked RB. 40 mg $NaBH_4$ was then added to the solution followed by stirring thoroughly. The RB was then fitted with a condenser, vacuumed and purged with Ar gas. It was then heated at 220 $^oC$ for 3 h. The product obtained was repeatedly washed with the hexane-ethanol mixture for several times and then dried in vacuum oven at 60 $^oC$ for 6 h.

### S4. Powder X-ray Diffraction (PXRD)

PXRD measurements were done at room temperature on a Rigaku Miniflex X-ray diffractometer with a Cu−$K\alpha$ X-ray source ($\lambda$ = 1.5406 Å), equipped with a position sensitive detector in the angular range of $10° \leq 2\theta \leq 90°$ with the step size 0.02° and a scan rate of 0.5 s/step calibrated against corundum standards. The experimental patterns were compared to the pattern calculated from the single crystal structure refinement.

### S5. Elemental Analysis

Quantitative microanalysis on all the samples was performed with an FEI NOVA NANOSEM 600 instrument equipped with an EDAX instrument. Data were acquired with an accelerating voltage of 20 kV and a 100 s accumulation time. The EDAX analysis was

performed using the P/B-ZAF standardless method (where Z = atomic no. correction factor, A = absorption correction factor, F = fluorescence factor, P/B = peak to background model) on selected spots and points. The composition was further confirmed by the ICP measurements using Perkin Elmer Optima 7000 DV instrument.

**S6. Transmission Electron Microscopy (TEM)**

TEM images and selected area electron diffraction (SAED) patterns were collected using a JEOL 200 TEM instrument. Samples for these measurements were prepared by sonicating the nanocrystalline powders in ethanol and dropping a small volume onto a carbon-coated copper grid.

**S7. X-ray Photoelectron Spectroscopy (XPS)**

XPS measurement was performed on an Omicron Nanotechnology spectrometer using a Mg−K$\alpha$ (1253.6 eV) X-ray source with a relative composition detection better than 0.1%.

**S8. X-ray Absorption Fine Structure Spectroscopy (XAFS)**

Pd *K*-edge XAFS measurements of $Pd_{17}Se_{15}$ nanoparticles were carried out in transmission mode at the P-65 beam line of the DESY-PETRA, Germany. *In-situ* Se *k*-edge XAFS data were collected at P-64 beamline of the DESY-PETRA, Germany. Pellets for the measurements were made by homogenously mixing the sample with an inert cellulose matrix to have an X-ray absorption edge jump close to one. Standard data analysis procedure was used to extract the extended X-ray absorption fine structure (EXAFS) signal from the measured absorption spectra. Background subtraction, normalization, and alignment of the XAFS data were performed by ATHENA software.[1] Theoretical EXAFS models were constructed and fitted to the experimental data in ARTEMIS.

The EXAFS fitting of ordered $Pd_{17}Se_{15}$ was done by taking the crystal structure of $Pd_{17}Se_{15}$.[2] Scattering paths were obtained by using FEFF6code. [1] EXAFS data of the catalyst materials were fitted simultaneously with *k*-weight of 1, 2 and 3. The $S_o^2$ value was fixed to 0.9 prior to the fitting procedure. The EXAFS data were Fourier transformed in the range of 4–13.8 $Å^{-1}$. Data were fitted in *R*-space between 1 and 3 Å for all the samples. The fitting parameters consist of bond length change between atoms ($\Delta R$), change in energy scale between data and theory ($\Delta E_o$) and mean-square displacement of the bond length ($\sigma^2$). The coordination numbers (*CN*s) were taken from the respective crystal structures and varied until low *R* factor was achieved.

**S9. Electrochemical Studies**

A three-electrode setup was used with a glassy carbon electrode with a diameter 3 mm as working electrode, platinum wire as counter electrode, and Ag/AgCl (1 M KCl) as

reference electrode. All the solutions were purged with nitrogen gas for 20 min prior to measurement. The catalyst ink was prepared by dispersing 1 mg of catalyst in 200 µL of mixed solvent solution (IPA: H2O = 1:1 v/v) and 10 $\mu$l of 0.05 wt % Nafion binder. The Nafion binder was diluted to 0.05 wt % with isopropyl alcohol (IPA). A 20 $\mu$l aliquot of the catalyst ink was drop casted onto a glassy carbon (GC) electrode and dried overnight at room temperature. Before depositing the catalyst, the GC was polished with 0.05 $\mu$m alumina slurry and washed several times with distilled water (18.2 MΩcm), and IPA. Commercial Pt/C (20 wt%, Sigma Aldrich) was used for comparison of activity with the **$Pd_{17}Se_{15}$** catalyst. The blank cyclic voltammetry (CV) measurement was carried out in 0.1 M KOH aqueous solution at a scan rate 50 mV/s. All the potentials shown here were referenced to the reversible hydrogen electrode (RHE).

The current-potential dependence of the reaction rate can be described by Koutecky-Levich (K-L) equation:

$$\frac{1}{j} = \frac{1}{j_k} + \frac{1}{j_d}$$

where $j$ is the measured current density ($mAcm^{-2}$), and $j_k$ and $j_d$ are the kinetic and diffusion limited current densities, respectively.

To further investigate the performance of the catalyst, linear sweep voltammetry measurements were carried out under an oxygen saturated 0.1 M KOH by sweeping the potential between 0 V and 1.1 V vs. RHE. The $J_d$ term can be obtained from the Levich equation:

$$J_d = \frac{Id}{A} = 0.62\ nFD^{2/3}\upsilon^{-1/6}\omega^{1/2}C_{O2}$$

where n is the number of electrons transferred, F is the Faraday's constant (96485 C $mol^{-1}$), A is the area of the electrode (0.0706 $cm^{-2}$), D is the diffusion coefficient of $O_2$ in 0.1 M KOH solution (1.9 x $10^{-5}$ $cm^2s^{-1}$), υ is the kinematic viscosity of the electrolyte (0.01 $cm^2s^{-1}$), ω is the angular frequency of rotation, $\omega = 2\pi f/60$, $f$ is the RDE rotation rate in rpm, and $C_{O2}$ is the concentration of molecular oxygen in 0.1 M KOH solution (1.2 x $10^{-3}$ mol $L^{-1}$).

For mass-transport corrected tafel plot, the kinetic current was calculated by:

$$j_k = \frac{j\,X\,j_d}{(j_d - j)}$$

The EIS was performed at a half-wave potential wih frequency sweep from $10^5$ – $10^{-2}$ Hz with a 5 mV AC amplitude. Stability test was carried out with graphite (>99.9 %) as the counter electrode to avoid Pt dissolution.

**S10. DFT Calculations**

All the calculations were carried out using Dmol$^3$ program. GGA-PBE functional was used to describe the electronic exchange and correlation effects. DND is chosen as the basis set with orbital cut-off of 3.5 Å. The convergence threshold values for energies, gradient and displacement are specified as 2 x $10^{-5}$ Ha, 5 x $10^{-3}$ Å, respectively, while the SCF convergence threshold is 1 x $10^{-5}$ Ha. Electron thermal smearing value of 0.005 Ha is employed for all the calculations to enhance SCF convergence efficiency. A vacuum slab of 10 Å was used to prevent any interaction with the neighbouring slab along *c* direction.

The binding energies for the systems under consideration were obtained from

$$Eb = E(ads/slab) – E(slab) - E(ads)$$

where E(ads/slab) is the energy of the final optimized adsorption configuration on the slab, E(ads) is the energy of the adsorbed molecule, and E(slab) is the energy of the catalyst (111) surface. With this definition, a negative Eb value corresponds to a stable adsorption on the surface.

## Tables:

**Table S1:** Composition determined by EDX and ICP of synthesized catalyst.

| **Method** | | ***Pd (at. %)*** | ***Se (at. %)*** |
|---|---|---|---|
| **EDX** | **Area 1** | ***40.93*** | ***59.07*** |
| | **Area 2** | ***43.70*** | ***56.30*** |
| | **Area 3** | ***47.53*** | ***52.47*** |
| | **Area 4** | ***46.58*** | ***53.42*** |
| | **Area 5** | ***44.42*** | ***55.58*** |
| **ICP** | **Sample 1** | ***47.22*** | ***52.77*** |
| | **Sample 2** | ***46.38*** | ***53.62*** |

**Table S2:** Refined parameters obtained from fitting EXAFS data.

| **Path** | **N** | **$S_0^2$** | **$\sigma^2$** | **$\Delta E_0$** | **Reff** |
|---|---|---|---|---|---|
| **Pd-Se** | 0.9+0.1 | 1.0 | 0.0005+0.0001 | 4.363+0.442 | 2.425+0.004 |
| **Pd-Pd** | 2.6+0.3 | 1.0 | 0.0040+0.0004 | 4.363+0.706 | 2.505+0.003 |

**Table S3:** Comparison of durability of catalyst synthesized in present work with that of literature.

| **Sl. No.** | **Catalyst** | **Stability technique** | **Duration** | **Loss** |
|---|---|---|---|---|
| 1. | Co/CoO on 3D N-rGO [3] | Chronoamperometry | 13000 sec | 2% |
| 2. | $MnO_2$/N-HGS [4] | Chronoamperometry | 12 h | 15% |
| 3. | Co-N-GCI [5] | Chronoamperometry | 20000 sec | 9.60% |
| 4. | Co/N/GR [6] | Chronoamperometry | 6 h | 27% |
| 5. | $ZnFe_2O_4$/rGO [7] | Chronoamperometry | 7000 sec | 18.50% |
| 6. | Co-NGX-900 [8] | Chronoamperometry | 10000 sec | 13% |
| 7. | $Co_3S_4$–S/G [9] | Chronoamperometry | 15000 sec | Slight decrease |
| 8. | $Cu_2ZnSnS_4$ [10] | Chronoamperometry | 40000 sec | Slight decrease |
| 9. | $MoS_2$/Pd [11] | ADT | 4000 Cycles | 0 shift |
| 10. | Pt/M-$TiO_2$ [12] | ADT | 4000 Cycles | 0 shift |
| 11. | $S_1N_5$-ordered carbon [13] | ADT | 1500 Cycles | 0 shift |
| 12. | Pt/CeOx/C [14] | ADT | 16000 Cycles | 0 shift |
| 13. | Pt_$Ti_3O_5$-Mo [15] | ADT | 5000 Cycles | 0 shift |
| 14. | $Pd_1Ru_1Ni_2$@Pt/C [16] | ADT | 10000 Cycles | 18.50% |
| 15. | P,N doped-HOPC [17] | ADT | 2000 Cycles | 14 mV shift |
| 16. | Pt/Vulcan [18] | ADT | 30000 Cycles | 53.3% |
| 17. | WC-$FeWO_4$@FeNOMC [19] | ADT | 10000 Cycles | 105 mV shift |
| 18. | $Pt_3Co$_Pt ultrathin shell [20] | ADT | 5000 Cycles | 0 shift |
| 19. | PtP [21] | ADT | 10000 Cycles | 5 mV shift |

| | | | | |
|---|---|---|---|---|
| 20. | $Co_7Se_8$ [22] | ADT | 1000 Cycles | 0 shift |
| 21. | Pt/PdAu [23] | ADT | 100000 Cycles | 8% shift |
| 22. | Rh doped Pt nanowires [24] | ADT | 10000 Cycles | 9.2% |
| 23. | $PtCuAu_{0.0005}$ [25] | ADT | 10000 Cycles | 8% |
| 24. | $Au/FePt_3/C$ [26] | ADT | 60000 Cycles | |
| 25. | $PtNi_3$ nanoframes [27] | ADT | 10000 Cycles | Slight decrease |
| 26. | This Work | ADT | 50000 Cycles | 11 mV positive shift |

**Table S4:** Refined parameters obtained from fitting EIS data.

| Circuit Element | Before Cycling | After 50K Cycles |
|---|---|---|
| **R1** | 110.6 ohm | 90.3 ohm |
| **Q1** | 0.162 mF | 0.238 mF |
| **R2** | 669 ohm | 775.9 ohm |
| **Q2** | 1.973 mF | 0.046 mF |
| **R3** | 398.8 ohm | 201.5 ohm |

**Table S5:** Refined fitting parameters of *in-situ* Se-*k* edge EXAFS data

| **$Pd_{17}Se_{15}$** | | | | | | |
|---|---|---|---|---|---|---|
| | **Paths** | **CN** | **$\sigma^2$** | **$E_0$** | **R (Bond Dist.)** | ***R*-factor** |
| ***Initial*** | ***Se-Pd*** | 3.32±0.09 | 0.005±0.0006 | 5.93±0.85 | 2.4629±0.005 | 0.009 |
| | ***Se-Se*** | 6.72±0.93 | 0.030±0.0140 | 5.93±0.85 | 2.8958±0.027 | |
| ***Dipped*** | ***Se-Pd*** | 3.24±0.08 | 0.005±0.0004 | 5.40±0.61 | 2.4628±0.003 | 0.009 |
| | ***Se-Se*** | 4.67±0.80 | 0.025±0.0109 | 5.40±0.61 | 2.9067±0.023 | |
| ***After ADT*** | ***Se-Pd*** | 3.13±0.01 | 0.005±0.0006 | 5.32±0.67 | 2.4698±0.004 | 0.014 |
| | ***Se-Se*** | 2.71±0.90 | 0.016±0.0095 | 5.32±0.67 | 2.9029±0.023 | |
| **$S_0^2$ =1** | | | | | | |

## Figures

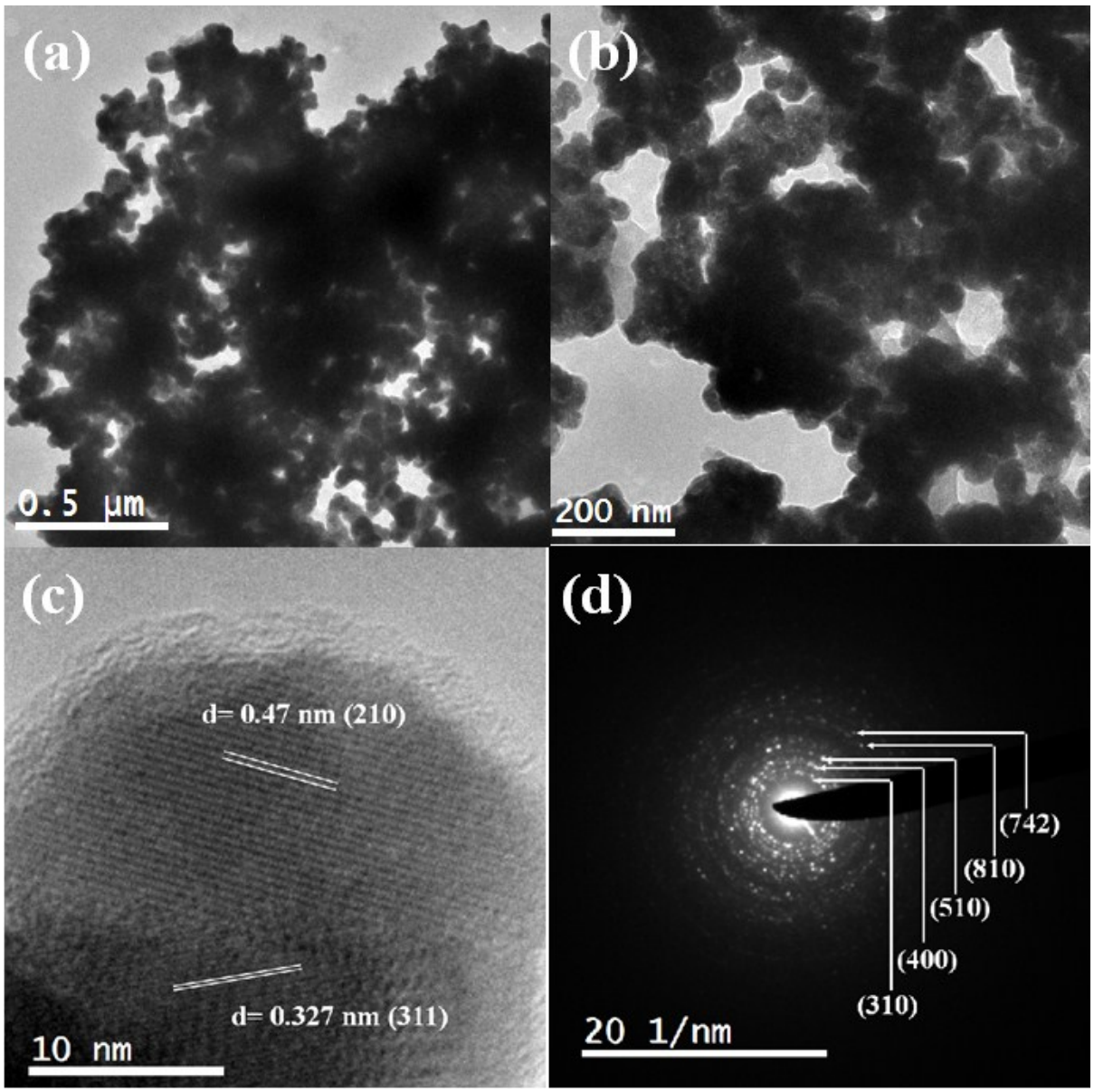


**Figure S1.** (a) TEM images shows the aggregated nature of the particle, (b) magnified TEM showing that the particles are interconnected, (c) HRTEM image shows the exposed (210) and (311) planes and (d) SAED pattern of $Pd_{17}Se_{15}$ nanoparticles shows polycrystalline nature of the nanoparticles.

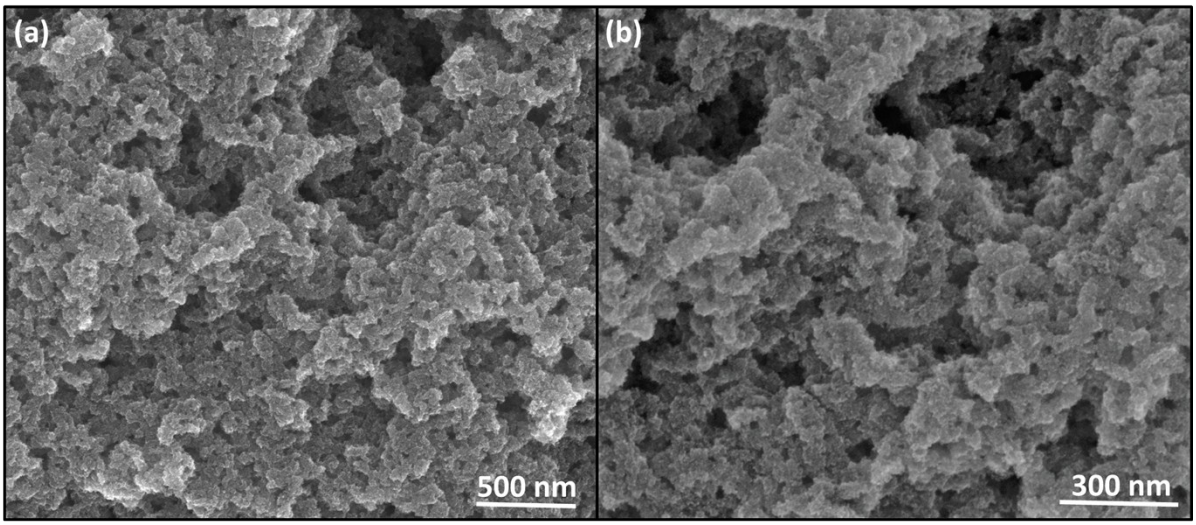


**Figure S2.** (a) Zoomed in and (b) zoomed out FESEM images of $Pd_{17}Se_{15}$ nanoparticles.

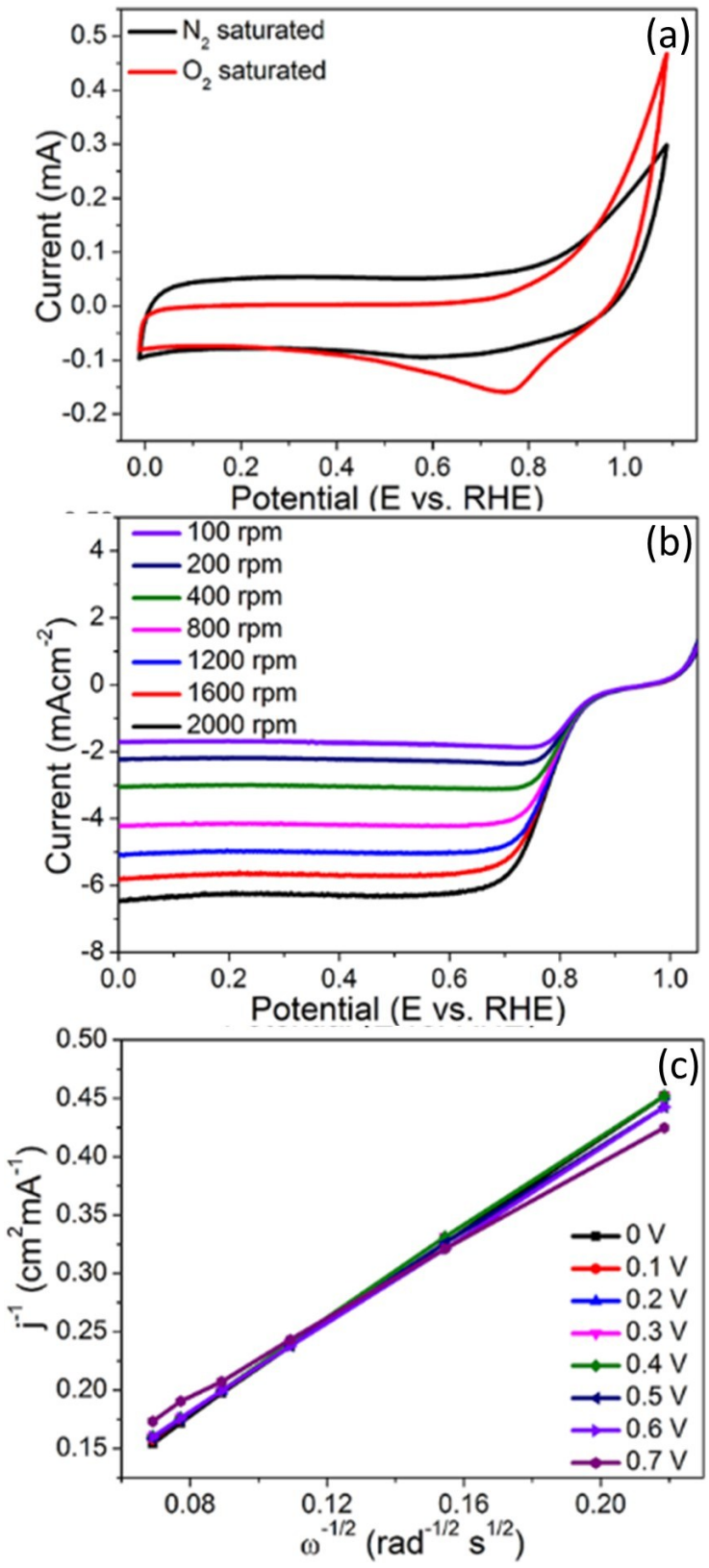


**Figure S3**. CV curve of the as-prepared sample in $N_2$ saturated (black line), and $O_2$ saturated (red line) 0.1 M KOH solution with a sweep rate of 50 mV/sec. Linear Polarization curves of $Pd_{17}Se_{15}$ at different rpm in 0.1 M KOH with a sweep rate of 5 mV/sec. Corresponding koutecky-levich (*K-L*) plot derived at a different potential.

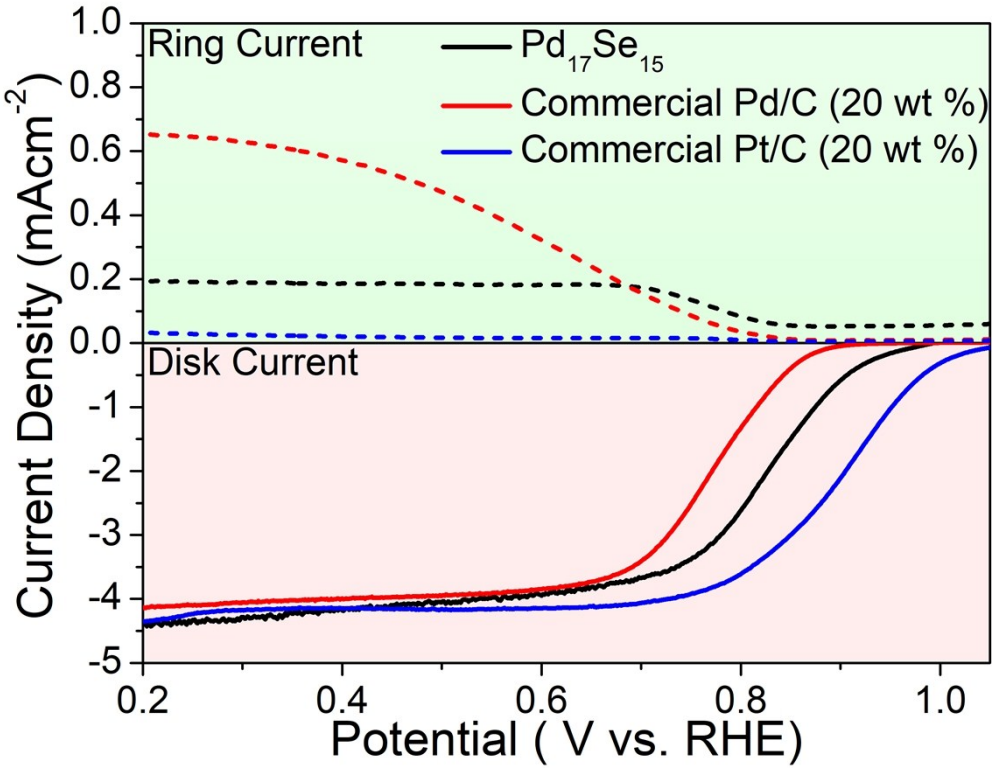


**Figure S4**. Comparison of ring and disk current of $Pd_{17}Se_{15}$ compared to that of commercial Pd/C and Pt/C.

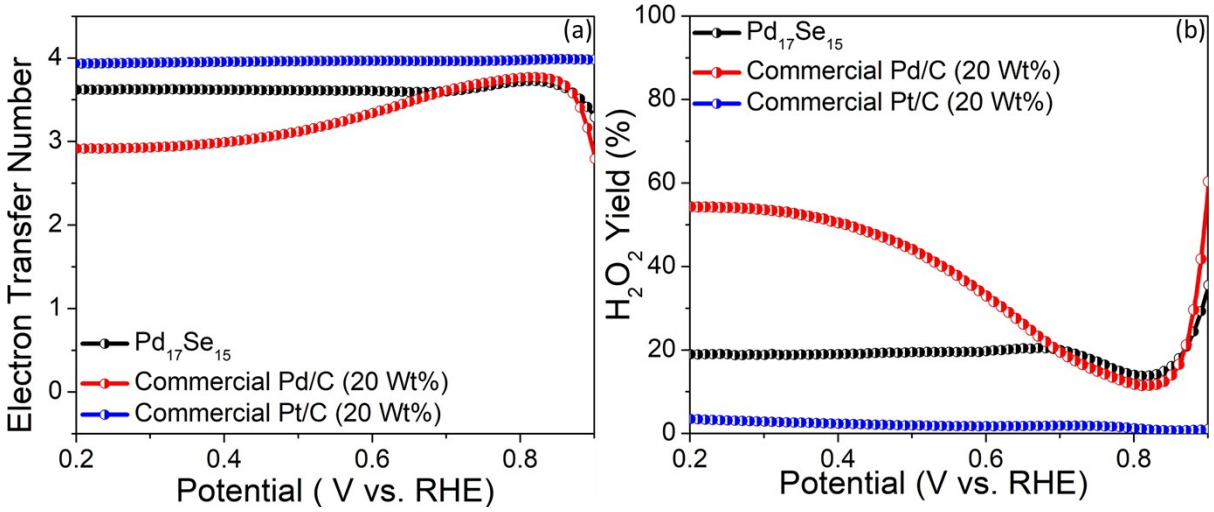


**Figure S5**. Comparison of the calculated electron transfer number and $H_2O_2$ yield with that of the commercial Pd/C and Pt/C catalyst.

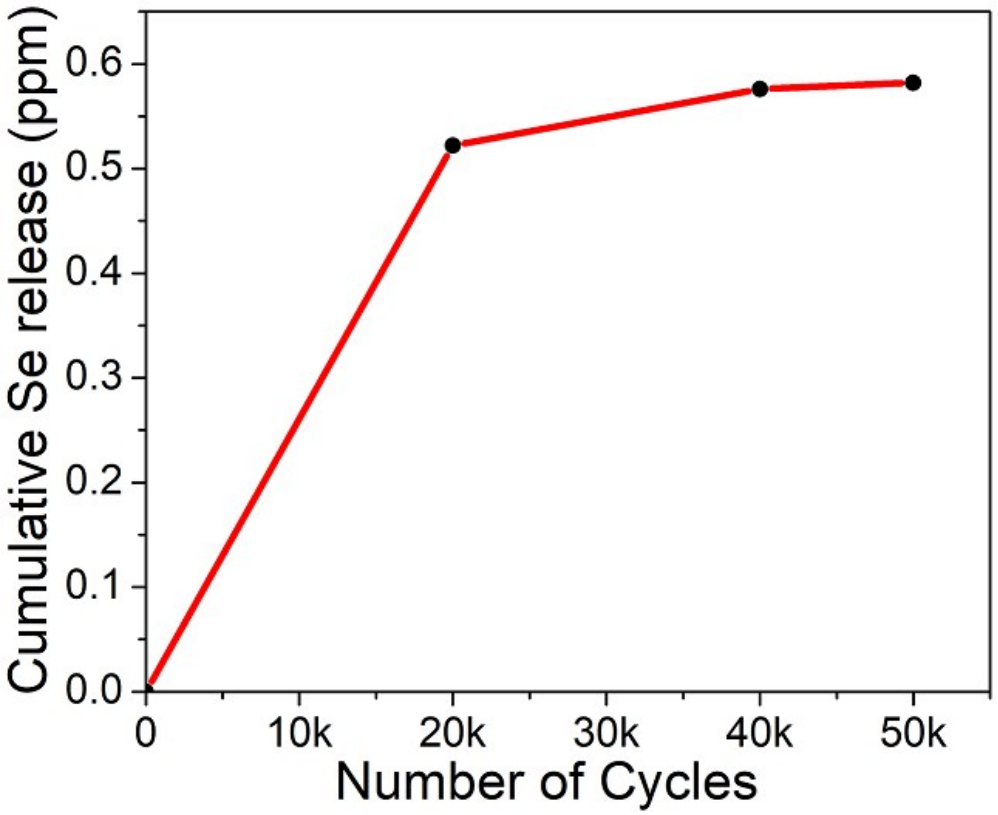


**Figure S6**. Cumulative selenium release curve of $Pd_{17}Se_{15}$ catalyst during prolonged cycling (50000 cycles) obtained from ICP-OES measurement.

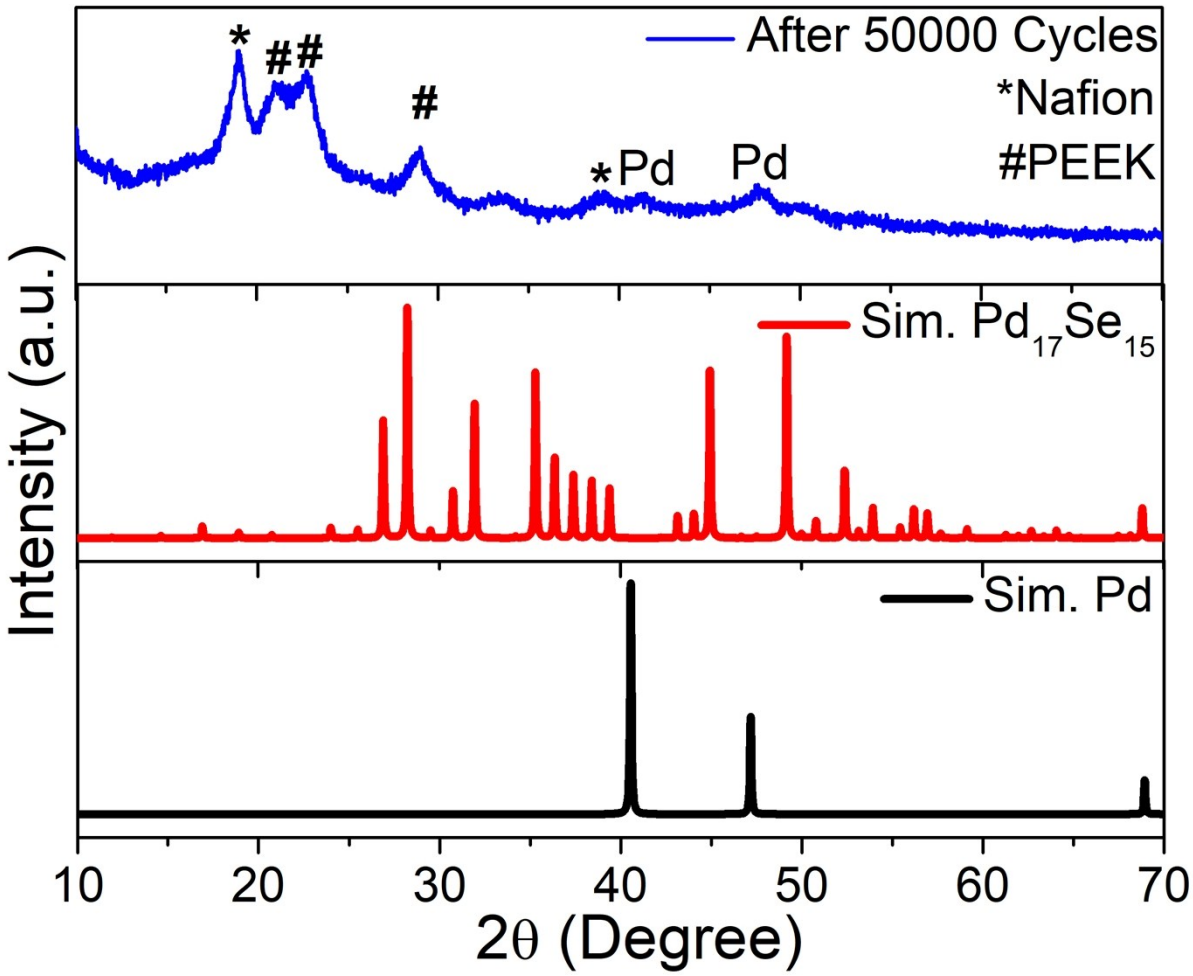


**Figure S7**. PXRD pattern of the catalyst after prolonged cycling (50000 cycles).

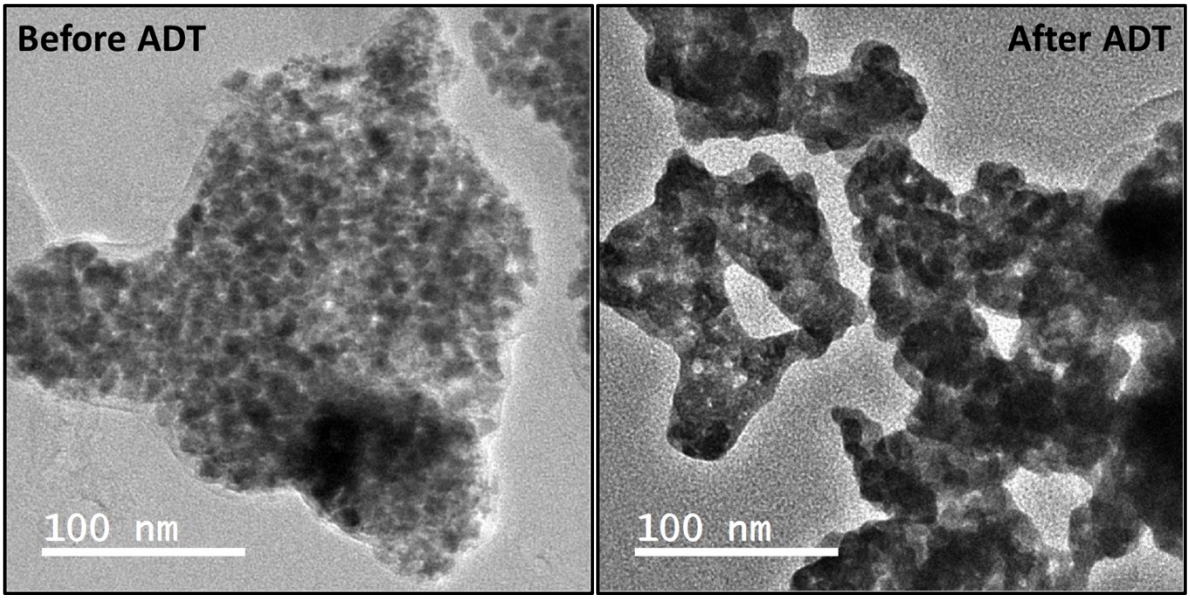


**Figure S8**. TEM images of the catalyst before and after prolonged cycling (50000 cycles).

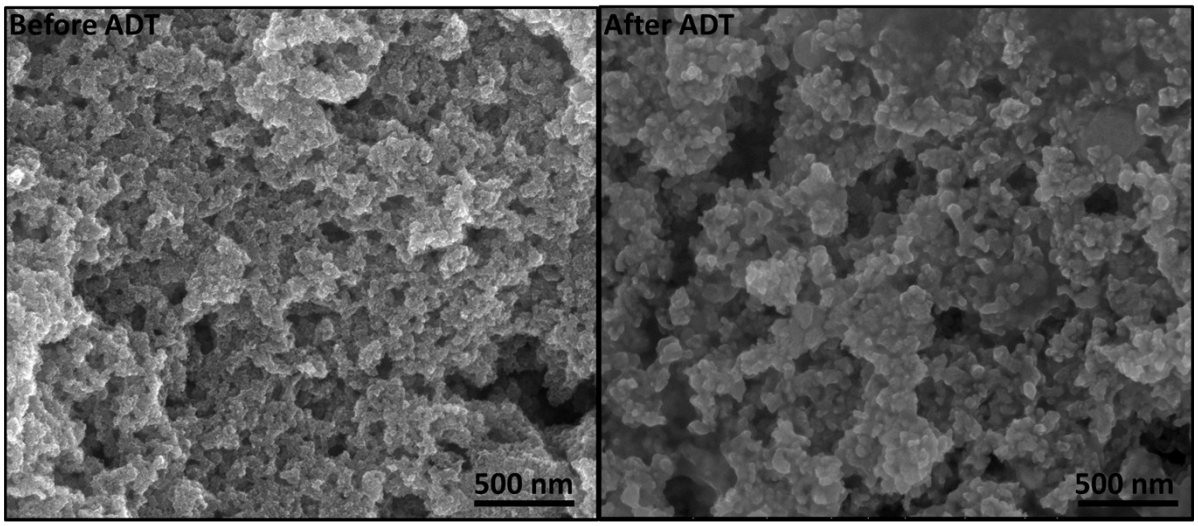


**Figure S9**. FESEM images of the catalyst before and after the stability test (50000 cycles).

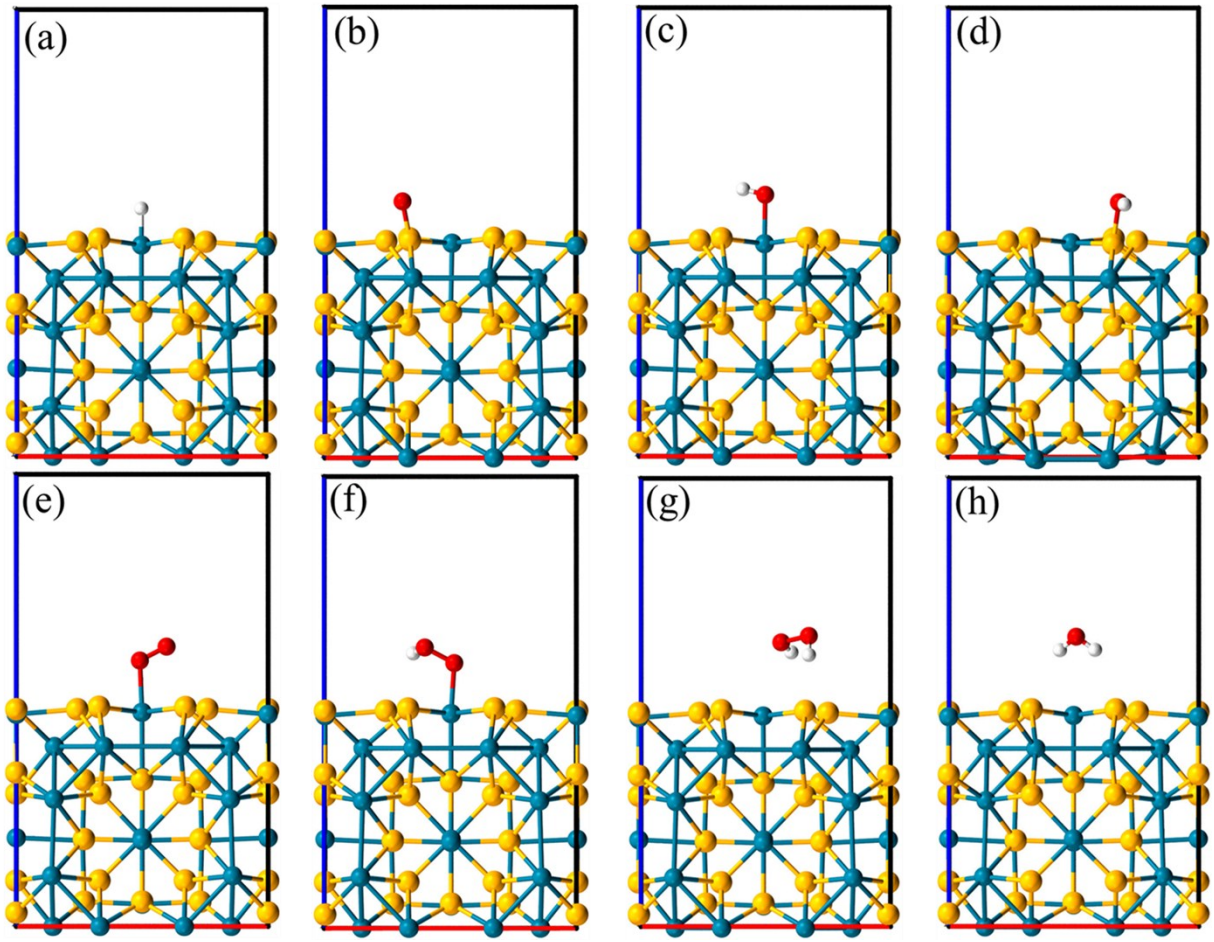


**Figure S10.** Stable adsorption configuration of (a) -H (b) –O, (c) –OH (Pd), (d)-OH (Se), (e) $O_2$, (f) –OOH, (g) $H_2O_2$ and (h) $H_2O$ on catalyst (100) surface. Blue, yellow, red and white coloured atoms represents Pd, Se, O and H atom respectively.

## References


1. B. Ravel, M. Newville, *J. Synchrotron Radiat.*, 2005, **12**, 537-541.
2. M. Yamauchi, T. Tsukuda, *Dalton Trans.*, 2011, **40**, 4842-4845.
3. M. Wang, Y. Y. Hou, R. C. T. Slade, J. Z. Wang, D. Q. Shi, D. Wexler, H. K. Liu, J. Chen, *Front. Chem.*, 2016, **4**.
4. Q. M. Yu, J. X. Xu, C. X. Wu, J. S. Zhang, L. H. Guan, *ACS Appl. Mater. Inter.*, 2016, **8**, 35264-35269.
5. X. C. Qiao, S. J. Liao, R. P. Zheng, Y. J. Deng, H. Y. Song, L. Du, *ACS Sustain. Chem. Eng.* 2016, **4**, 4131-4136.
6. J. W. Liang, M. Hassan, D. S. Zhu, L. P. Guo, X. J. Bo, *J. Colloid. Interf. Sci.*, 2017, **490**, 576-586.
7. W. Hong, L. Z. Li, R. N. Xue, X. Y. Xu, H. Wang, J. K. Zhou, H. L. Zhao, Y. H. Song, Y. Liu, J. P. Gao, *J. Colloid. Interf. Sci.*, 2017, **485**, 175-182.
8. D. L. Yu , X. Q. He, *J. Appl. Electrochem.*, 2017, **47**, 13-23.
9. W. L. Gu, L. Y. Hu, W. Hong, X. F. Jia, J. Li, E. K. Wang, *Chem. Sci.*, 2016, **7**, 4167-4173.
10. X. L. Yu, D. Wang, J. L. Liu, Z. S. Luo, R. F. Du, L. M. Liu, G. J. Zhang, Y. H. Zhang, A. Cabot, *J. Phys. Chem. C*, 2016, 120, 24265-24270.
11. L. X. Zuo, L. P. Jiang, J. J. Zhu, *Ultrason. Sonochem.*, 2017, **35**, 681-688.
12. J. H. Kim, G. Kwon, H. Lim, C. Zhu, H. You, Y. T. Kim, *J. Power Sources*, 2016, **320**, 188-195.
13. T. T. Jiang, Y. Wang, K. Wang, Y. R. Liang, D. C. Wu, P. Tsiakaras, S. Q. Song, *Appl. Catal B-Environ.*, 2016, **189**, 1-11.
14. Y. Luo, L. Calvillo, C. Daiguebonne, M. K. Daletou, G. Granozzi, N. Alonso-Vante, *Appl. Catal B-Environ.*, 2016, **189**, 39-50.
15. R. A. M. Esfahani, S. K. Vankova, A. H. A. M. Videla, S. Specchia, *Appl. Catal. B-Environ.*, 2017, **201**, 419-429.
16. H. X. Nan, X. L. Tian, J. M. Luo, D. Dang, R. Chen, L. N. Liu, X. H. Li, J. H. Zeng, S. J. Liao, *J. Mater. Chem. A*, 2016, **4**, 847-855.
17. C. W. Deng, H. X. Zhong, X. F. Li, L. Yao, H. M. Zhang, *Nanoscale* 8 (2016) 1580-1587.
18. B. Z. Fang, B. A. Pinaud, D. P. Wilkinson, *Electrocatalysis-Us*, 2016, **7**, 336-344.
19. K. Wang, Y. Wang, Y. X. Tong, Z. W. H. Pan, S. Q. Song, *ACS Appl. Mater. Inter.*, 2016, **8**, 29356-29364.
20. Z. Y. Li, R. Zeng, L. G. Wang, L. J. Jiang, S. M. Wang, X. P. Liu, *Int. J. Hydrogen Energ.*, 2016, **41**, 21394-21403.
21. L. L. Zhang, M. Wei, S. Q. Wang, Z. Li, L. X. Ding, H. H. Wang, *Chem. Sci.*, 2015, **6**, 3211-3216.
22. J. Masud, M. Nath, *ACS Energy Lett.*, 2016, **1**, 27-31.
23. K. Sasaki, H. Naohara, Y. M. Choi, Y. Cai, W. F. Chen, P. Liu, R. R. Adzic, *Nat. Commun.* 2012, **3**.
24. H. Huang, K. Li, Z. Chen, L. Luo, Y. Gu, D. Zhang, C. Ma, R. Si, J. Yang, Z. Peng, J. Zeng, *J. Am. Chem. Soc.*, **2017**, 139, 8152-8159.
25. B. A. Lu, T. Sheng, N. Tian, Z. C. Zhang, C. Xiao, Z. M. Cao, H. B. Ma, Z. Y. Zhou, S. G. Sun, *Nano Energy*, 2017, **33**, 65-71.
26. C. Wang, D. van der Vliet, K. L. More, N. J. Zaluzec, S. Peng, S. H. Sun, H. Daimon, G. F. Wang, J. Greeley, J. Pearson, A. P. Paulikas, G. Karapetrov, D. Strmcnik, N. M. Markovic, V. R. Stamenkovic, *Nano Lett.*, 2011, **11**, 919-926.
27. C. Chen, Y. J. Kang, Z. Y. Huo, Z. W. Zhu, W. Y. Huang, H. L. L. Xin, J. D. Snyder, D. G. Li, J. A. Herron, M. Mavrikakis, M. F. Chi, K. L. More, Y. D. Li, N. M. Markovic, G. A. Somorjai, P. D. Yang, V. R. Stamenkovic, *Science*, 2014, **343**, 1339-1343.